Univerzita Karlova v Praze
Přírodovědecká fakulta

HABILITAČNÍ PRÁCE

RNDr. Ing. Martin Kalbáč, Ph.D.

Isotopic labeling and in situ Raman spectroscopy in graphene research

Praha, 2018

Prohlášení
Prohlašuji, že jsem tuto závěrečnou práci zpracoval samostatně a že jsem uvedl všechny použité informační zdroje a literaturu.
V Praze dne 8.října 2018.

Poděkování: Rád bych poděkoval manželce Janě za její morální i odbornou pomoc. Dále bych chtěl poděkovat všem svým kolegům, kteří se podíleli na realizaci prezentovaných výsledků.

Table of content

1 Introduction

Single-layer graphene (1-LG) is the archetype two-dimensional (2-D) material. It comprises a one-atom-thick layer of carbon atoms, which are assembled into a honeycomb-like lattice. Because of its fascinating properties, the graphene has inspired many experimental and theoretical works. It has also a large potential for plethora of advanced applications in optoelectronics, nanoelectronics, sensors, *etc*. Although this material is very simple by means of its crystal structure, there are still many open questions regarding its properties, which need to be explored. As the 1-LG represents a standalone surface, its interaction with surroundings strongly influences its band structure - the position of the Fermi level and distortion of the Fermi surface - thus the coveted physical properties.

Recently, the attention has focused on controlled stacking of graphene layers and other 2-D crystals giving rise to the unique class of materials termed van der Waals heterostructures. In general these systems are more versatile than 1-LG with respect to their formability and thus application possibilities. On the other hand, they are also more complex and more difficult to study; the great challenge is to disentangle the response of the individual graphene layers in such systems. The graphene bilayers are the most simple, but the most fascinating case among the few-layer van der Waals structures. Depending on the mutual orientation, their properties can be tuned from Mott insulating state over non-interacting regime to unconventional superconductivity at the so-called magic angle orientation.[1] In this work, we demonstrate how to address the structural and electronic properties of the individual graphene layers using a unique concept of isotope labeling and in situ Raman spectroscopy, which has the power to address these challenges in the research of 2-D materials.

The habilitation thesis is structured as follows. After a brief Introduction (section 1), the summary of our work on preparation and physiochemical properties of 1-LG are presented (section 2-3). In particular, section 2 is devoted to the studies of 1-LG and to the influence of external stimuli (doping, strain and interaction with substrate) on this material. In the section 3, the two layer graphene (2-LG) is discussed as a model structure for multilayer graphene systems and several examples of the study of these materials using isotope labeling are given, including study of the growth, addressing of the doping and heating effects, functionalization and defects in individual layers. In addition application of graphene in surface enhanced Raman spectroscopy and graphene in sandwiched structures are discussed. Conclusions and

outlooks are given in section 4. The thesis is completed with the references (section 5) and list of the publications. For readers convenience the references co-authored by M. Kalbac are emphasized in bold in the text. Finally, the collection of the publication is presented in section 6.

2 Single-layer graphene

2.1 Preparation of graphene samples

Graphene can be prepared by several approaches. The first graphene samples were prepared by mechanical exfoliation from bulk graphite.[2] Although this method provides high-quality graphene samples, it is not applicable for large-scale production of graphene. Therefore, other scalable methods were developed. Among those methods, chemical vapor deposition (CVD) is the most promising.[3] Figure 1 shows a schematic picture of the CVD reactor. In this case, the carbon source (usually methane) together with hydrogen gas is introduced into the furnace and heated to about 1000 ºC. In addition, the synthesis of graphene requires a catalyst. The most used catalysts are nickel and copper metals. These two catalysts exhibit different mechanisms of the graphene growth process: In the case of Ni, the precursor gas is decomposed at the surface and carbon is dissolved in the metal. When the substrate is cooled, the solubility of C in Ni decreases and graphene first segregates and then grows on the Ni surface. Hence, it is very important to control the cooling conditions to obtain monolayer graphene (1-LG).[4] On the other hand, in the case of the copper catalyst, the carbon intermediate is not dissolved in the metal because the solubility of C in Cu is negligible even at a very high temperature. Instead, the carbon atoms form graphene directly on the surface already at high temperature, i.e., there is no need to precisely control the cooling of the metal. CVD on copper is suggested to be surface mediated and self-limiting. Once the monolayer is completed, the process does not propagate any more, because the catalytic Cu surface is blocked. Hence, only 1-LG should be formed by the Cu-catalyzed CVD. Nevertheless, in many cases, small regions with double- or multilayers are typically observed. The mechanism of the formation of multilayer regions was unclear until recently. These multilayer regions may impede the fabrication of graphene devices on a large scale because the multilayer areas disturb the uniformity of the graphene film. Despite a recent progress in the CVD graphene synthesis the domain size is limited to hundreds of micrometers, hence there is still a long

way to reach a large-scale production using such a method. In addition, such procedures seem to require extremely clean conditions and long growth time, which would make the growth expensive. It was also suggested that the epitaxial growth copper (111) leads to a uniform high-quality monolayer.[5] Nevertheless, the use of single crystals for the graphene growth would be difficult to scale up. Based on the results obtained from our study, a different approach can be suggested. Because the slowly growing layers are located on top of the faster-growing ones, they are well accessible for etchants. In addition, the slowly growing layers have accessible reactive edges, which are more susceptible to the etching. If a multilayer-free 1-LG is required, it is thus possible to etch away the multilayers. In fact, such an etching step can be interfaced with the growth. Hence, the multilayer-free graphene can be prepared by a simple hydrogen etching, which follows immediately after the methane source was turned off while still maintaining both the hydrogen flow and also the temperature used for the growth. This shifts the equilibrium toward hydrocarbons' formation and the multilayers are etched away.

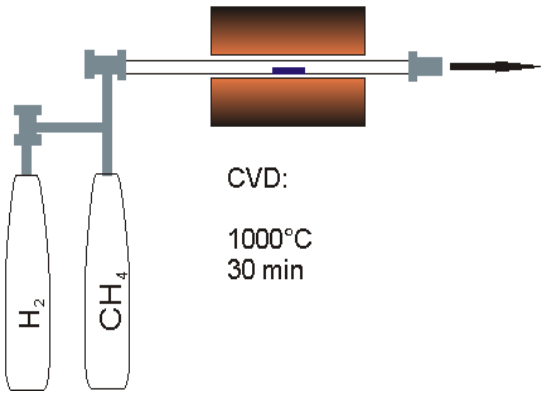

Figure 1. The chemical vapor deposition process used for the preparation of graphene.

Copper foil is not ideal for identification and further characterization of graphene. Nevertheless, graphene can be transferred onto other substrates, typically on SiO_2/Si substrate (with 300 nm oxide layer). So far, many different approaches to transfer graphene have been reported, among them the transfer process using poly(methyl methacrylate) (PMMA) is the most popular.[6] In the latter case, the graphene is covered by a thin layer of a solution of

PMMA and after drying of the solvent, the copper foil is dissolved in iron(III) chloride, resulting in a graphene with PMMA floating on a liquid. The graphene can then be “fished” by a substrate of choice. Finally, the PMMA layer is removed using acetone or by a thermal treatment in a hydrogen atmosphere.

2.2 Raman spectroscopy of (single-layer) graphene

Raman spectroscopy is the most widely used tool to study and characterize graphene samples. It allows distinguishing between one- or two-layered graphene, it can provide information about defects in graphene, about doping of graphene or mechanical strain in graphene.

The unit cell of graphene contains two carbon atoms, which gives six phonon modes. Of those modes, three are acoustic (A) and three optical (O). Both acoustic and optical phonon branches consist of one out-of-plane vibration (o) and two in-plane vibrations (i). The in-plane vibration can be parallel (L) or perpendicular (T) to the line connecting two nearest carbon atoms. Because of the phonon momentum conservation requirement, the first-order Raman features originate from the close vicinity of the Γ point in the first Brillouin zone of graphene. The iTO and iLO phonon branches merge at the Γ point and give rise to the G mode of graphene. In other words, the G mode originates from a double generate (E_{2g}) phonon mode.

Figure 2 shows a typical Raman spectrum of graphene excited using 2.33 eV laser excitation energy. The Raman spectrum of graphene consists of two important bands: the G and the 2D mode (also called G′ mode in the literature). If the sample contains defects then also the D mode is present in the spectra. As mentioned, the G band in the Raman spectrum originates from the zone center E_{2g} phonon mode and in undoped samples it is found at about 1580 cm^{-1}. The D and 2D modes are observed in the spectral regions of 1250–1450 cm^{-1} and 2500–2900 cm^{-1}, respectively. The 2D mode and the D mode (in case of defects) are observed in all kinds of polycrystalline carbon materials with sp^2 hybridization. However, their physical origin has been explained only recently by double-resonance theory.[7] The selection rules for electron–phonon scattering allows activation of the iTO phonon connecting electronic states near the K and K' points. This intervalley process gives rise to the 2D mode.

The one-phonon second-order Raman D-band appears only if there is a breakdown in translational crystal symmetry, which can be caused by defects in the structure. On the other hand, the two-phonon second-order Raman 2D feature occurs independently of the presence of structural defects. The two phonons contributing to the 2D feature have wave vectors **q** and –**q**, and thus the momentum conservation constraint is automatically preserved. The D mode is important for the quantification of defects in graphene. (Note that there is another defect-related feature - D′ mode - originating from the intravalley process. The D′ mode is located at about 1610 cm^{-1}, hence it is overlapping with the G mode, especially in the case that the sample is doped. Therefore, the D′ mode is typically not analyzed unless the number of defects is large.)

Because of the double-resonance nature of D and 2D modes, their Raman signal reflects both the electronic structure of graphene and phonon dispersion relations in graphene, consequently both the D and the 2D Raman mode exhibit dispersive behavior. Hence, when a different laser excitation energy is used, a phonon with a different **q** vector and different energy is employed in the resonance process.

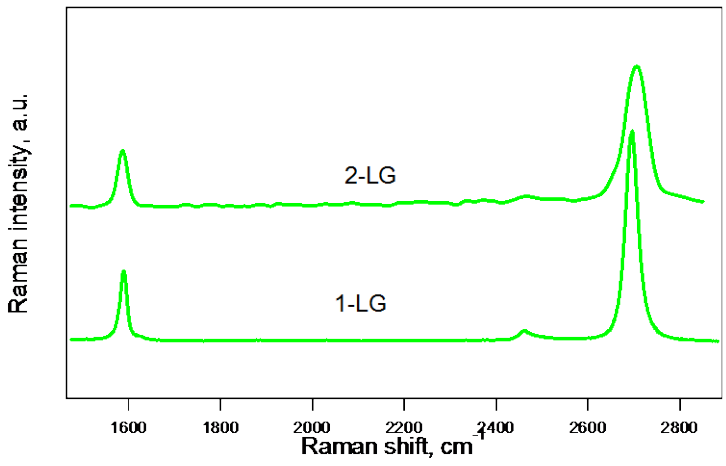

Figure 2. The Raman spectra of the 1-LG and AB-2-LG.

2.3 Changing properties of graphene by external stimuli

The properties of graphene can be externally manipulated essentially by two methods: application of strain and doping. Both strain and doping of graphene can be applied reversibly and they can be followed in situ by Raman spectroscopy. Graphene samples are usually studied on substrates. The substrates can cause strain and doping of graphene, and in some cases, there is even a possible mixing of electronic states of graphene and the specific substrates. Therefore, the substrate plays a crucial role in the studies of graphene and low-dimensional materials in general.

2.3.1 Doping of graphene studied by Raman spectroscopy

Electrochemical or electrostatic doping provides an easy way to control the Fermi level of graphene, which makes these methods attractive for applications[8,9]. However, the electrostatic doping depends on the properties of the dielectric. The doping efficiency is typically very low, and for this reason, a high voltage (up to 100 V) must be used. In addition, the doping is complicated by the presence of trapped charges in the dielectric serving as a substrate[10]. Electrochemical doping, on the other hand, is more efficient, so that a voltage of ±1.5 V is usually sufficient to reach a significant doping and consequently a pronounced shift of the Fermi level.[11] The latter method, so-called in situ Raman spectroelectrochemistry, allows monitoring the changes in the electronic structure of different materials during electrochemical doping. Because the Raman spectra of graphene and graphene-based low-dimensional systems are strongly affected by doping, in situ spectroelectrochemistry is an ideal method for studies of these systems in a charged state.[12]

Both the G and the 2D modes frequencies shift and change their intensity upon doping (Figure 3). The frequency shift of the G band in charged graphene is related to the change in the C–C bond strength and to the renormalization of the phonon energy.[13] In graphene, a coupling between lattice vibrations and Dirac fermions is allowed because the scales for the electron and phonon dynamics are comparable. Therefore, the adiabatic Born–Oppenheimer approximation fails to describe the G band phonons. Hence, time-dependent perturbation theory is needed to explain the experimental observations. The carriers in graphene interact with phonons and electron–hole pairs are created. This leads to a renormalization of both the

phonon energy and the energy of the carriers. In charged graphene, the Fermi energy E_F is moved away from the Dirac point and thus the formation of electron–hole pairs is suppressed.[13] Because of electron–hole symmetry with respect to the Dirac point, the frequency shift of the G mode should be identical both for positive and negative doping. However, the doping also induces a change of the C–C bond strength.[9] The positive doping removes the electrons from antibonding orbitals and therefore a hardening of the phonon corresponding to the G band is expected. On the other hand, negative doping adds electrons to the antibonding orbitals, which should lead to a softening of the Raman signal frequency (ω_G). Both phonon energy renormalization and a change of the bond strength occur and the two effects are superimposed in the experimental Raman spectra. For positive doping, both effects lead to an upshift of the phonon frequency. However, for negative doping, they have an opposite effect on the frequency shift. This is consistent with the experimental results because a monotonic increase of the G band frequency was found at positive electrode potentials and a non-monotonic change in frequency was observed for negative electrode potentials. In addition, the observed shift of the G band frequency never becomes as large for the negative potentials.

The behavior of the 2D (G') mode frequency ω_{2D} is also sensitive to doping.[8,11] An increase in ω_{2D} with increasing magnitude of the positive electrode potentials is usually observed. On the other hand, for electron doping, there is first an increase in ω_{2D}, followed by a relatively large decrease in ω_{2D}. The change Δ of ω_{2D} with respect to the electrode potential ($\Delta\omega_{2D}/\Delta V$) includes the effects of changes in the C–C bond strength, the electron–phonon coupling and electron–electron interactions. Similarly, as in the case of ω_G, the hole doping increases ω_{2D} and electron doping decreases ω_{2D}.

The Raman intensities of both the G and 2D modes of graphene also exhibit a significant dependence on electrode potential. The signal intensity of the 2D band is monotonically decreased as the magnitude of the electrode potential is increased, both for positive and negative potential values. For the G band, a more complex behavior is found. The interesting feature in the case of positive doping is a dramatic increase of the Raman G band intensity at high positive electrode potentials.[11,14] The enhancement of the Raman signal at high positive potentials is counterintuitive; nevertheless, it is consistent with recent theoretical work by Basko.[15] His calculation suggests that the matrix element for the G band increases when the

Fermi level is close to $E_{laser}/2$. It is also obvious that if the laser excitation energy decreases then the Fermi level will reach $E_{laser}/2$ at lower magnitudes of electrode potentials. The enhancement of the G mode intensity observed is a consequence of the latter situation.

In contrast to the complex intensity *vs.* potential profiles of the G band, the 2D band exhibits a monotonic decrease of the intensity for both positive and negative doping. It has been suggested previously[16] that the intensity of the 2D band (I_{2D}) is proportional to the electron/hole inelastic scattering rate. Doping increases the number of charge carriers and therefore the probability of a scattering event increases and the 2D band intensity, therefore, decreases.[16]

Strong doping of graphene layers and sandwiches is crucial for substantial changes of their electronic properties required by applications in electronic devices.[17] However, a strong doping is difficult to achieve. The charge induced by electrostatic gating is limited by the dielectric layer. The electrochemical doping is more successful to reach high doping levels. Nevertheless, in the case of graphene, it is also limited by the stability of the system. Recently, a new method, which enables to increase the available potential range significantly has been developed.[18] The approach is based on the formation of a protective layer which prevents degradation of graphene at high electrode potentials. An optimized composition of the protective layer allows achieving both strong doping level and simultaneous measurement of the Raman spectra. Raman spectroscopy measurements are crucial because these measurements allow evaluation of the doping level of graphene and also to study the formation of defects in graphene. In other words, by Raman spectroscopy one can estimate the real change in the doping level of graphene and also identify the doping level when the graphene starts to degrade. The successful protective layer contained one layer of poly(allylamine hydrochloride) and one layer of poly(acrylic acid). The protective layer also allowed using a liquid nonaqueous electrolyte with high doping efficiency. We have shown that by the proposed method one can reach very high doping levels. Alternatively, the strong doping can be realized by applying an electrode potential to the ferroelectric polymer layer deposited on graphene.[19]

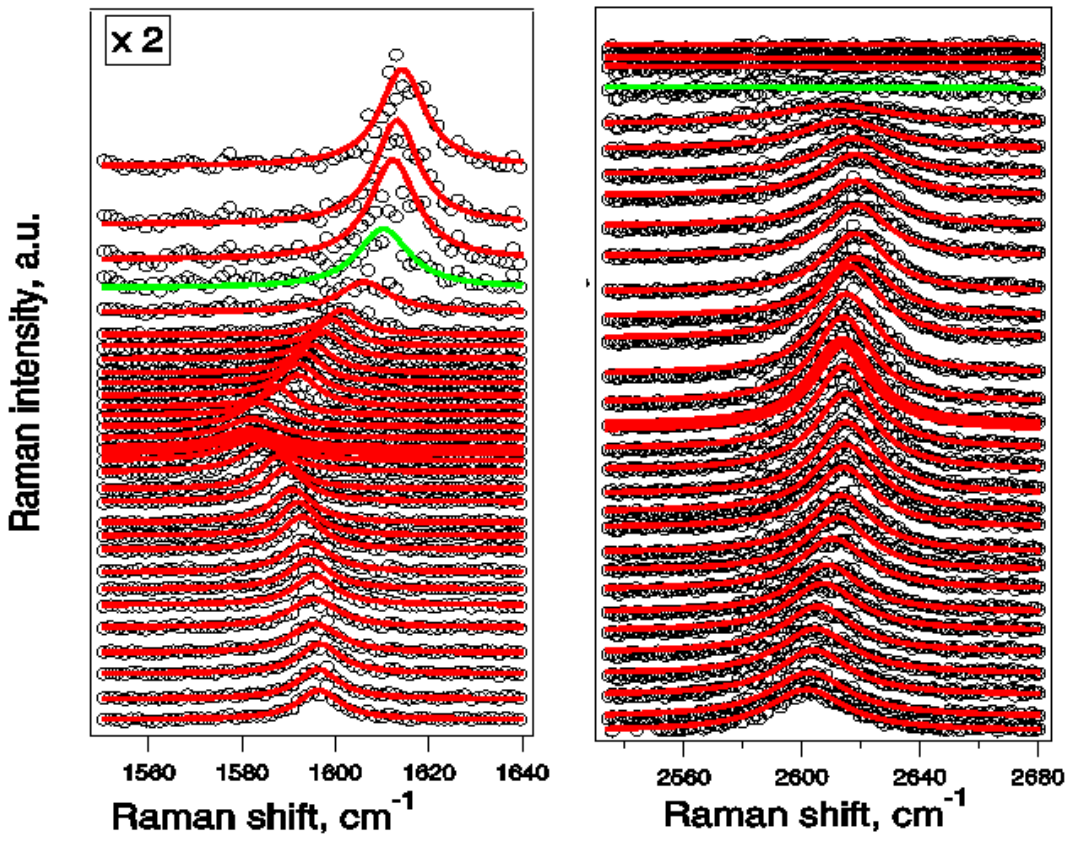

Figure 3. In situ Raman spectroelectrochemistry of 1-LG, the figure was adopted from Ref.[11]

2.3.2 Strain in graphene

In general, Raman spectroscopy can be applied to identify and quantify the strain in graphene. The strain can be uniaxial, biaxial or triaxial or combined.[20] The strain changes the strength of the carbon bonds and also the electronic structure. Furthermore, it has been demonstrated that strained graphene can mimic the electronic structure like it would be placed in a giant external magnetic field.[21] The strain manifests itself both in the frequency of the G and 2D modes. The changes in the G mode are relatively small hence the G mode is not usually used to identify the strain in graphene. Larger changes are observed in case of the 2D mode. Nevertheless, also the 2D mode is dependent on the doping, therefore, one needs to decouple the effects of the doping and the strain.

2.3.3 Doping and strain disentanglement

As discussed above, the G mode frequency is very sensitive to doping and less sensitive to strain, on the other hand, the 2D mode frequency is very sensitive to strain and only slightly sensitive to doping. Because the G and the 2D mode exhibit a different sensitivity to doping and strain, it is possible to extract the changes in strain and doping in graphene samples even if both effects are present simultaneously. For a proper analysis of strain and doping in graphene samples it is necessary to measure Raman maps and from the obtained data construct correlation plots of the 2D and G mode frequencies.[22] Assuming biaxial strain only, the slope of ω(2D)/ω(G) is 2.45. The slope of the ω(2D)/ω(G) line caused by doping only is 0.7. In case that the graphene experiences zero doping and zero strain ω(G) = 1582 cm^{-1} and ω(2D) = 2674 cm^{-1} (using 532 nm laser excitation). This point can be used as an origin for the strain and doping lines. The experimental set of points is then placed onto the same graph and one can read the strain and the doping from strain and doping lines which are crossing at a particular experimental point.

An alternative approach is to analyze the 2D′ mode. The frequency of the 2D′ mode has been shown to depend strongly on the strain, while the dependence on the doping is negligible.[23] On the other hand, the intensity of the 2D mode is relatively weak, hence this approach can be used only if the Raman signal of the sample is strong, for example in the case of graphene on SiO_2/Si.

2.3.4 Interactions with the substrate

As discussed above, Raman spectroscopy is an efficient tool to study the doping and strain in graphene. Consequently, Raman spectroscopy is also very useful to study substrate–graphene interactions because these interactions are usually dominated by charge transfer and strain. Graphene samples are grown on copper metal hence, it is straightforward that the graphene–copper interactions are very important and need to be further investigated. We studied graphene grown by chemical vapor deposition on copper single crystals with exposed (100), (110) and (111) faces.[24] Our examination of the as-grown graphene by Raman spectroscopy using a range of visible excitation energies and micro-Raman mapping showed distinct strain and doping levels for individual Cu surfaces. By comparison of the results from Raman mapping with X-ray diffraction techniques and Atomic Force Microscopy, it was shown that

the Cu lattice orientation is responsible for the specific strain and doping values in graphene. This was in contrast to previous expectation, where the crystal quality or the surface topography was suggested to be the main parameter influencing graphene–Cu interactions. It was also found that an exceptionally narrow Raman 2D band width is caused by the interaction between graphene and the metallic substrate. The appearance of this extremely narrow 2D band with full-width-at-half-maximum (FWHM) as low as 16 cm^{-1} was correlated with flat and undoped regions on the Cu(100) and (110) surfaces. The generally compressed (~0.3% of strain) and n-doped (Fermi level shift of ~250 meV) graphene on Cu(111) showed the 2D band FWHM minimum of ~20 cm^{-1}. The graphene grown on Cu foil under the same conditions reflects the heterogeneity of the polycrystalline surface and its 2D band was accordingly found to be broader with FWHM > 24 cm^{-1}. The graphene is grown at a very high temperature (about 1000 ºC) and then the sample is cooled to room temperature. In other words, the as-grown graphene experiences large temperature changes, which also results in strain generation because of the different thermal expansion coefficients for copper and graphene. The changes in temperature and strain presumably affect the copper–graphene interactions. Therefore, another desirable experiment is in situ Raman spectroscopy during heating of the graphene grown on copper single crystals. This approach has been demonstrated to be a simple method for estimating and manipulating the level of interaction between graphene and copper single crystals through heat treatment. We performed in situ Raman spectroscopy showing Cu face-specific behavior of the overlying graphene during the heat treatment. On Cu(111), the interaction is consistent with theoretical predictions and remains stable, whereas, on Cu(100) and Cu(110), the initially very weak interaction and charge transfer can be tuned by heating. Our results also suggest that graphene grown on Cu(100) and Cu(110) is detached from the copper substrate, thereby possibly enabling an easier graphene transfer process as compared with Cu (111).[24,25]

For several applications and studies, the graphene is transferred onto a different substrate. The most used substrate is Si/SiO_2. The transfer process typically involves a heating step to remove the transfer polymer or to clean the transferred graphene. On the other hand, for the measurement of the electrical properties of graphene, the samples are cooled to helium temperature. Therefore, it is very important to understand the changes in graphene–substrate interactions in dependence on changes of the temperature. For example, in the case of Si/SiO_2 substrate, it was shown the graphene–substrate interactions are strongly affected by a

presence of water at their interface. Figure 4 shows a plot of the Raman frequency of the G mode in dependence on temperature. The sample was followed during two temperature cycles.[26] Before heating the G mode position is about 1580 cm^{-1}, which corresponds to neutral graphene. During the first heating cycle, the frequency of the G mode decreases due to temperature-induced changes in C–C bond length and phonon–phonon interactions.[27] These changes are fully reversible, therefore, after cooling the sample back to room temperature, the G mode position should return to 1580 cm^{-1}. However, the G mode position after the first temperature cycle is found at about 1590 cm^{-1}, which suggests a slight doping of the graphene sample. The G mode position during the second heating step follows precisely the cooling part of the first temperature cycle. The changes in the G mode position during the cooling part of the second temperature cycle matches the changes during the heating part of the second temperature cycle, hence the changes are now fully reversible. The observed effect is rationalized by the presence of water at the interface between graphene and substrate. The water is removed by heating the sample, which results in tighter contact of graphene and substrate and therefore the graphene becomes more doped. The water is removed already by the first temperature cycle, therefore the second temperature cycle is reversible. Note that for complete removal of the water from the graphene SiO_2/Si interface, temperatures of above 500 K are necessary.

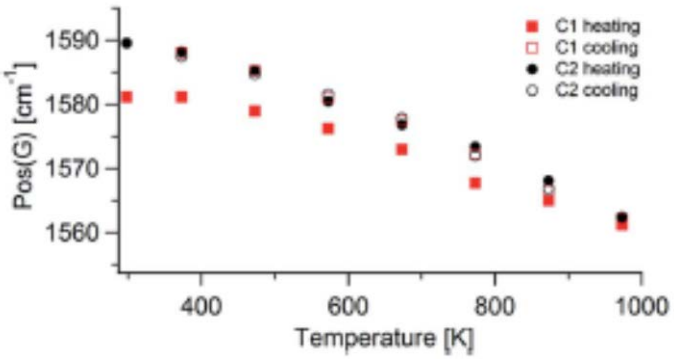

Figure 4. The changes in the shift of the G mode frequency during two thermal cycles, the figure was adopted from Ref.[26]

For more detailed analysis, Raman maps of the samples heated to 573 K and 973 K were studied. Figure 5 shows the distribution of the G mode frequencies before and after annealing. The histograms show that the doping of graphene is similar after heating to 573 K and 973 K, which means that at 573 K the water is completely removed. The changes in the temperature may also lead to changes in the strain. To disentangle the effects of the strain and

doping, the G and 2D frequencies at each particular Raman spot were extracted and plotted in Figure 5b. It can be seen that the points before annealing are located in the region of the neutral and unstrained graphene. After annealing, the experimental data points are located further along the doping line, which confirms doping of the sample. In addition, for the sample heated to 973 K, the points are also located close to the strain line, which suggests substantial strain induced by the heating cycle. The strain was estimated as 0.13% (compressive). The compression of the sample can be rationalized by a mismatch of the temperature expansion coefficients of graphene and substrate. While during the cooling the silicon substrate shrinks, the graphene expands.

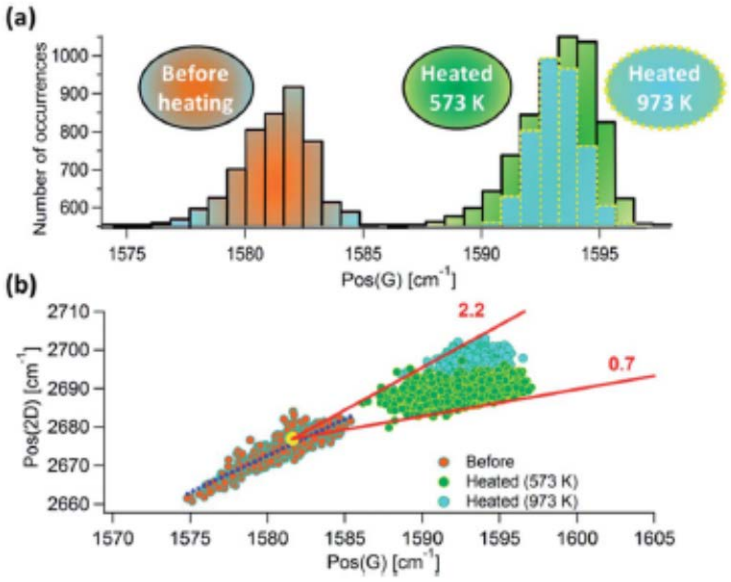

Figure 5. Top: histogram of the G mode frequencies obtained from Raman mapping of the untreated graphene sample, the sample heated at 573 K and the sample heated at 973 K. Bottom: strain/doping analysis of the untreated graphene sample, the sample heated at 573 K and the sample heated at 973 K. The figure was adopted from Ref.[26]

Low-temperature treatment probed down to 50 K showed that graphene is influenced predominantly by changes in the graphene and substrate dimensions.[28] While the Si/SiO_2 substrate shrinks, the graphene lattice expands. This leads to compressive strain, which is in this case relaxed by the formation of wrinkles. In the wrinkle area, the sample detaches from the substrate, which leads to a decrease in the doping level of graphene. Consequently, local

inhomogeneities in the doping of the samples are created. This is an important finding, which has to be considered when characterizing the sample by low-temperature measurements.

For a specific application, the substrate can be selected so that the properties of graphene are tuned by changes in the properties of the substrate or by changes of external conditions, for example, temperature. For example, $BaTiO_3$ (BTO) undergoes several thermoelastic martensitic phase transitions when it is cooled from 300 K to 10 K. Consequently, graphene, which is transferred onto BTO is subjected to significant changes in strain at these phase transitions.[29] The doping is also different due to a large dielectric constant and spontaneous polarization of the BTO, which changes at different phases and ferroelectric domains of BTO.

3 Graphene multilayers

The multilayer graphene represents a step toward more complex 2-D materials. The simplest and most widely studied representative of this new class of 2-D materials is bilayer graphene. As compared with single-layer graphene, the bilayer graphene has a new free parameter, which is the orientation of the layers with respect to each other. In general, random orientation is called turbostratic bilayer (T-2-LG) and the special case when the carbon of one layer are located just above the center of the hexagons of the second layer is called AB-stacked or Bernal-stacked bilayer (AB-2-LG). The orientations of the layers reflect in the changes of the electronic structure. This change is the most obvious for the AB-stacked 2-LG. Nevertheless, as was demonstrated recently, also the specific orientation of the layers leads to the formation of van Hove singularities in the electronic structure of graphene[30] giving rise to the superconducting or Mott insulating states at very low angles.[1] Because the orientation of graphene layers can be arbitrarily set, these results open a path to realize devices with tunable electronic structure.

The multilayers of graphene with a defined number of layers can be prepared by subsequent transfer of one graphene layer on top of another graphene layer(s). The bilayers prepared by the transfer method are typically turbostratic as they do not follow the order of layers in graphite. Nevertheless, recently it was shown that the angle between the layers can be finely

tuned by using a specialized transfer stage. For AB-stacked graphene, one can apply the modified condition of the CVD protocol, which leads to the formation of bilayer/multilayers.

3.1 Isotope labeling

Raman spectroscopy can be used to distinguish between 1-LG and AB-2-LG. In Figure 2, there is shown the Raman spectrum of 1-LG together with the spectrum of AB-2-LG. As can be seen, the spectra are very similar. The only difference is broadening and change in symmetry of the 2D mode of the AB-2-LG as compared with the 1-LG. In the case of T-2-LG, the spectra typically do not differ from the spectrum of 1-LG. (However, for some specific angles between graphene layers one can observe a strong enhancement of the Raman signal due to resonance with van Hove singularities).[30] For in any case, it is not possible to distinguish the signal coming from the top and bottom layers of 2-LG. Using $^{13}CH_4$ in CVD growth one can prepare ^{13}C graphene. Because of the higher mass of the ^{13}C isotope, the Raman frequency of graphene features is shifted to lower frequencies following the simple equation:

$$(\omega_0 - \omega)/\omega_0 = 1 - [(12 + c_0)/(12 + c)]^{1/2}$$

where ω_0 is the frequency of a particular Raman mode in the ^{12}C sample, $c = 0.99$ is the concentration of ^{13}C in the enriched sample, and $c_0 = 0.0107$ is the natural abundance of ^{13}C.

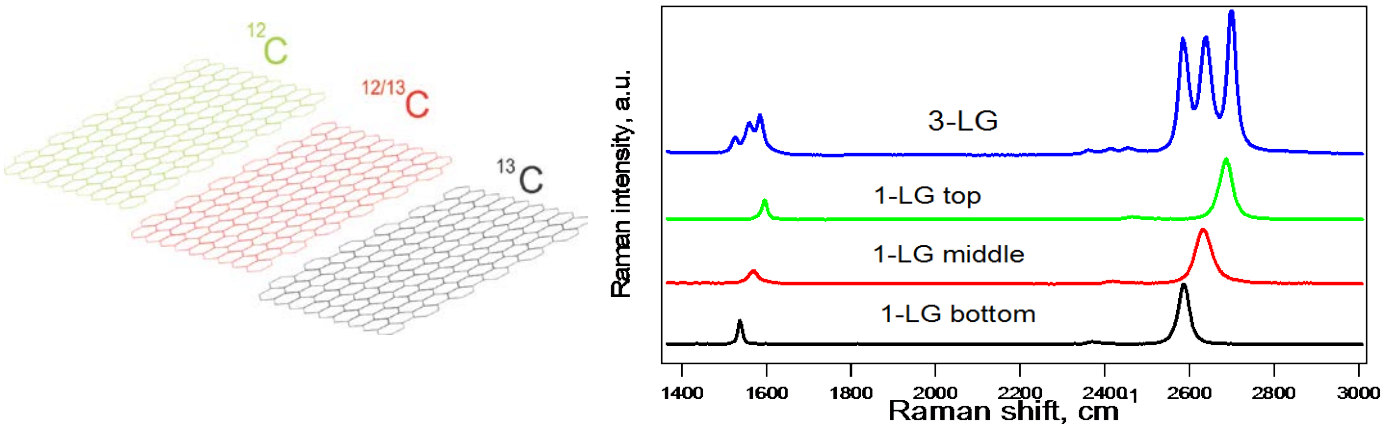

Figure 6. The Raman spectra of the ^{13}C graphene, $^{12/13}C$ graphene, ^{12}C graphene and isotopically labeled 3-LG. The figure was adopted from Ref.[31]

Now, if we compose the 2-LG from the ^{12}C layer and ^{13}C layer, it is possible to distinguish the top and the bottom layers of 2-LG.[32,33] This simple approach can be further extended for studies of multilayer graphene. For such a case, graphene layers with different isotope combinations must be prepared and combined. For example, in the case of three-layer graphene, the ^{12}C, ^{12}C+^{13}C (1:1) and ^{13}C graphene layers will be combined as shown in Figure 6.[31]

Isotope labeling enables new experiments, which will not be possible without this technique.[34] In the following chapter, a few examples of such studies are shown.

3.2 Study of multilayer graphene growth mechanism

Isotope engineering provided us a unique possibility for advanced studies on graphene growth by Raman spectroscopy. In our study, we used either ^{13}C or ^{12}C methane as the carbonaceous precursor to follow the Cu-catalyzed CVD synthesis of graphene in detail. Based on these results, we succeed to modify the growth conditions to suppress the presence of double layers.[35] To analyze the growth, we measured the Raman spectra profiles across the graphene grain grown initially from $^{13}CH_4$ and subsequently from $^{12}CH_4$, see Figure 7. We found that the Raman bands indicating the carbon isotope content were altered across the grain. In the central area, the Raman spectra consist only of the contribution of ^{13}C graphene with intensities twice as high as in the rest of the grain. Because $^{13}CH_4$ was used at the beginning of the growth, the exclusive contribution of ^{13}C to the doubled intensity in the center of graphene grains suggests that the second layer is formed already at the initial stages of the growth. Therefore, middle 2-LG region of the grain actually corresponds to the initial graphene seed. Going slightly off the center of the graphene grain, the contribution of ^{12}C graphene in addition to the signal of ^{13}C graphene starts to be apparent with their overall intensity still being at the level of the initial ^{13}C bands. The signal of ^{12}C graphene again disappears at the border of the central 2-LG region and, at the same time, the signal intensity of ^{13}C is reduced by about 50% compared with the signal intensity in the central 2-LG area. Going further in a direction toward the grain edge, the signal of ^{12}C graphene appears again, together with the ^{13}C signal vanishing, and remains constant until the grain boundary. The presence of ^{12}C in the double-layer part of the sample means that these regions grow during

the whole growth, but obviously slower than the dominating single-layer part of the graphene grain. In other words, the top and bottom layers grow independently. An important practical consequence of this observation was that prolonging the time of the growth would also lead to an increased size of the multilayer regions if there is still a free copper surface. If the copper surface is fully covered by graphene, also the top layers stop to grow or this growth is suppressed because there are no carbonaceous intermediate precursors available. Consequently, the formation of a complete double- or multilayer is limited.

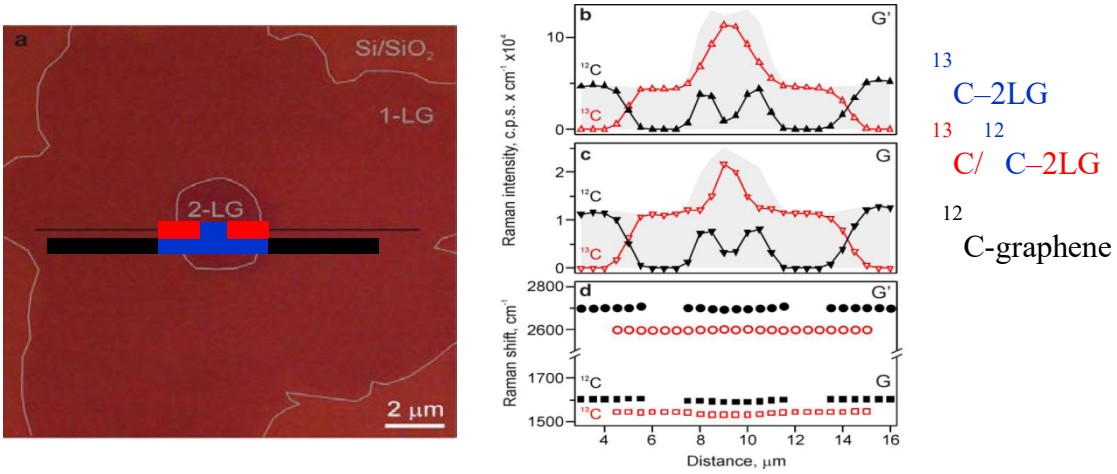

Figure 7. Growth and measurement of the isotopically labeled AB-stacked bilayer graphene. a) Optical image of the 2-LG grain. b) Plot of the G mode intensity vs. the distance from the grain center. c) Plot of the G′(2D) mode intensity vs. the distance from the grain center. d) Plot of the G and G′(2D) mode frequencies vs. the distance from the grain center. The figure was adopted from Ref.[35]

The stacking order of graphene layers in the graphene bilayer can also be confirmed by Raman spectroscopy. Figure 8 shows Raman spectra of turbostratic 2-LG and the AB-stacked 2-LG. For both AB and turbostratic graphene layers, one can find two G modes, corresponding to the top and bottom graphene layers. However, the appearance of the 2D mode is different. While in the case of turbostratic 2-LG there are two modes, in the case of AB-stacked 2-LG only one broad band is found. This can be rationalized by considering the number of phonons involved in the Raman process. For the G mode, there is only one phonon mode involved. It can originate either from the top or bottom layer, which defines its position

in the Raman spectrum. The Raman process responsible for the 2D mode involves two phonons. Consequently, there are three possible combinations: both originate from the bottom layer, both originate from the top layer, one originates from the top and the second from the bottom layer. The two former cases give rise to two Raman 2D modes. If the latter case is possible, then there should be one additional band in between the bands of the top and bottom layers. The intensity of this band is expected to be two times larger than the intensity of the peak corresponding to the process were phonons from only one layer are involved. In the case of the turbostratic 2-LG graphene, the interaction between layers is weak as compared with the interaction between graphene layers in AB-stacked 2-LG. Therefore the "middle" peak is expected to appear only in the case of AB-stacked 2-LG. In reality the 2D mode consists of four subbands, nevertheless, all of them can be identified and assigned using isotope labeling.[36]

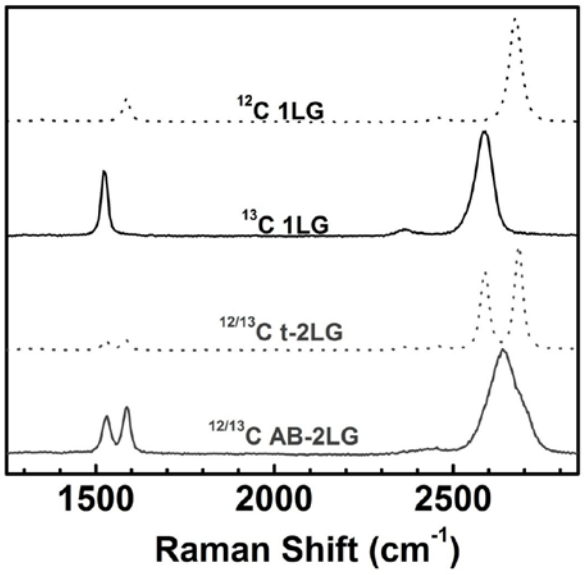

Figure 8. Raman spectra of ^{12}C, ^{13}C 1-LG and isotopically labeled T-2-LG and AB-2-LG. The figure was adopted from Ref.[37]

3.3 Doping of multilayered graphene

The properties of the two-layered graphene (2-LG) can also be altered by doping. In fact, a specific doping of AB-stacked 2-LG leads to opening of the bandgap in this material, which is crucial for applications in electronic devices. Because of the importance of doping for practical applications like transistors, there is a need to study the effects of doping in detail.

One of the open questions is related to the distribution of the charge between graphene layers in doped 2-LG. This problem can be addressed by Raman spectroscopy as the Raman features of graphene strongly depend on the doping level. To distinguish between the top and bottom layer we employed an isotopically labeled 2-LG in which one layer was of natural isotope composition (mostly of ^{12}C atoms) and the second layer is labeled by the ^{13}C isotope. The isotopic labeling allowed us to follow the Raman spectra of the two components (the top and bottom layers) of bilayer graphene separately (Figure 9). In our work, we focused on analyzing the changes in the Raman intensity of the G and 2D bands as a function of the electrode potential. In the case of the T-2-LG, the changes of the signal with electrode potential are almost the same for both layers, which means that the doping level of graphene layers in T-2-LG is the same at all applied electrode potentials.[38] In addition, the observed changes are similar to those observed in 1-LG during the doping. This reveals that graphene layers in T-2-LG behave like two independent materials. These results provide a new insight into a charge transfer between graphene sheets, which is also potentially very useful for the interpretation of the results obtained on carbon nanotubes and carbon nanostructures in general.

Isotope labeling also allows studying the role of stacking order on the doping. It is very interesting that if the graphene layers are AB stacked, the charge transfer process between the graphene layers is completely different as compared with the turbostratic graphene samples.[37] As can be seen in Figure 9, there is a significant difference between the behavior of the shift of the G mode with increasing electrode potentials. The experimental results demonstrated a nonequivalent charge distribution between graphene layers in doped AB-stacked graphene bilayers. As the applied potential is increased, the G mode of the bottom layer stays almost unchanged, while the G mode of the top layer is shifted toward higher frequencies. This indicates that more charge is located at the top layer than at the bottom layer. In AB-2-LG, the electrochemical charging also reflects a smaller sensitivity of Fermi level to the electrode potential due to the effect of the modified electronic structure as compared with that for T-2-LG.

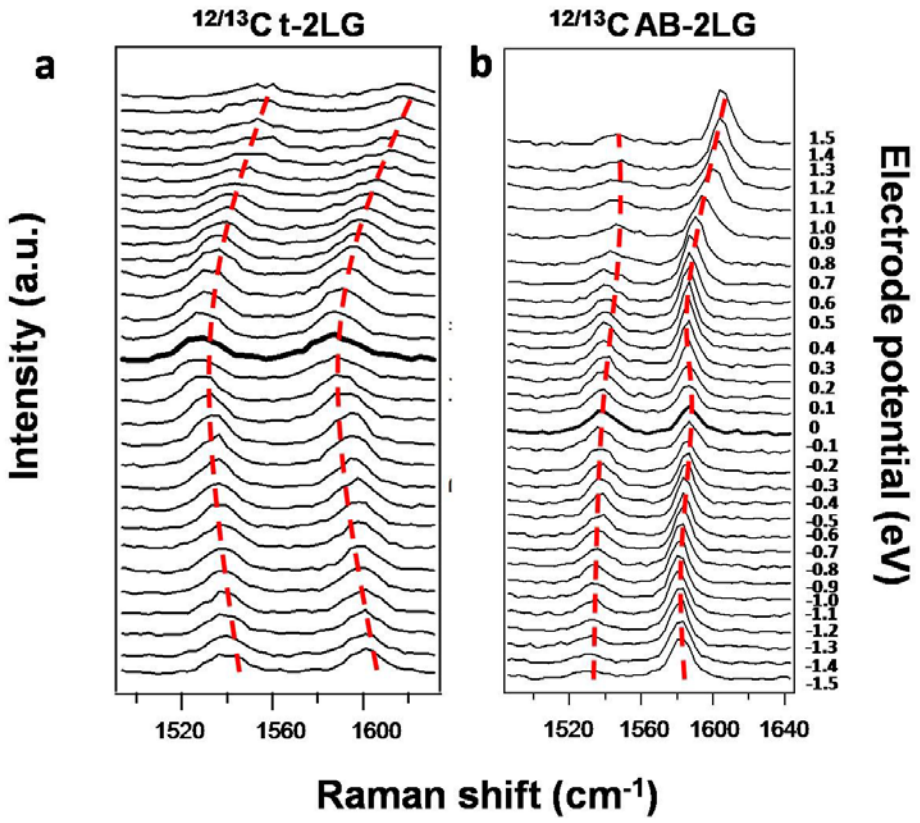

Figure 9. In situ Raman spectroelectrochemistry of a) T-2-LG and b) AB-2-LG. The potential step is 0.1 V.[37]

In some cases, the direct contact of graphene and the electrolyte needs to be avoided. One option to avoid such a contact is the use of ferroelectric polymers. The study of the doping behavior of graphene was focused on the influence of the gradual polarization of a ferroelectric polymer on isotopically labeled 2-LG. Predominantly, Raman spectroscopy was used to analyze the effect of the polarization. The Raman frequencies of the ^{13}C graphene modes were downshifted with respect to the Raman frequencies of ^{12}C graphene, which enabled us to study the individual layer components of 2-LG. The polarization of the ferroelectric polymer showed similar influence on the electron and hole concentrations at the ^{13}C graphene and the ^{12}C graphene layers despite the ^{13}C graphene layer being only in direct contact with the ferroelectric polymer. In this experiment the specific doping of graphene was confirmed by similar frequency shifts of the G modes and similar changes in the intensities of the 2D modes during the electrochemical charging of the ferroelectric polymer. Consequently, our experimental results suggested that the behavior of the graphene during

charging is influenced predominantly by changes in electrostatic potential and also confirms that graphene can be efficiently doped by the polarized ferroelectric polymer. In addition, this finding could be useful for applications, where long-term stability of doping is required.

3.4 Heating of graphene and graphene bilayers

The isotope labeling can be used also to study the behavior of graphene bilayer during thermal treatment.[39] Two-layer graphene may be a working element in new types of electronic devices. The current driven through graphene generates heat in a device. Therefore, it is very important to study the effects of heating on graphene. Although there are several studies reporting on 1-LG, the studies on multilayered graphene are very rare. The use of isotope engineering is very efficient to study the effects of environment on 2-LG. The tested 2-LG samples were composed of a ^{12}C layer (contacting the substrate) and ^{13}C graphene layer (on top of the ^{12}C layer). The changes observed in the Raman spectra during thermal treatment were attributed mainly to the change in the mechanical stress of graphene. The changes were found to be significantly stronger for the bottom layer than for the top layer due to a strong interaction of the bottom layer with the substrate. The behavior of both directly synthesized turbostratic and AB-stacked bilayers was also compared.[40] It was found that the coupling between the two layers is strong for both stacking orders, despite the fact that turbostratic grains still show separate signals for the two layers, with intensities similar to monolayer graphene. In fact, a small difference can be observed between the layers in T-2-LG and AB-2-LG samples during heating. These findings differ from the ones obtained for bilayers constructed by subsequent transfer of two single layers of graphene, where the layers were found to be decoupled with the top layer floating freely on top of the bottom layer.

3.5 Defect formation and analysis

Another example of the application of isotope labeling is the study of defect formation in 2-LG. As in conventional semiconductors, atomic-scale defects in graphene strongly influence its properties and may have either detrimental or overall beneficial effects on the characteristics of the material. Examples of the former are a decrease in electron mobility or

drop in mechanical characteristics with an increase in defect concentration. To study the defect formation in 2-LG, it is necessary to use isotope labeling. In this case, the isotopically engineered single and bilayer graphene sheets are used as ion irradiation targets. The samples are formed by subsequent transfer of ^{12}C and ^{13}C graphene sheets on Si/SiO_2 substrate and irradiated by Ar^+ ions with various doses.[41] Raman spectroscopy was used to assess the amount of damage in the samples. The approach based on isotope labeling allows distinguishing the effects of ion bombardment on different graphene sheets. The number of defects created in graphene by Ar^+ ion bombardment is evaluated by monitoring the changes in the Raman spectra of the samples and estimating the ratio of D/G and D/G′ mode intensities. Contrary to theoretical estimates based on the conventional binary collision model, which is routinely used nowadays for assessing irradiation damage in bulk materials, the experimental results indicate that the number of defects in the bottom layer of the bilayer graphene sample is smaller than in the upper layer. The discrepancy can be understood in terms of an enhanced rate of defect annealing in the lower layer, as confirmed by a simple analytical model based on the results of analytical potential molecular dynamics simulations. Hence, these results indicated that annealing of defects in two-dimensional materials may be particularly important and can be thus useful when irradiation is used to tailor the properties of graphene and other 2D systems.

Another important problem in the case of multilayer graphene samples is related to the size of the area affected by defects. In the case of 1-LG, it was shown that the effects of defects can be seen at about 1.8 nm away from their location.[42] As the distance between graphene layers in a bilayer is about 0.335 nm one can raise a question, whether the defect is also affecting nearby layers. The defects in graphene can be generated selectively in the top layer. In this case, oxygen plasma can be used. If the conditions are appropriately adjusted, one can generate single atom defects. The defect creation can be monitored by Raman spectroscopy. As discussed above in the case of bilayer graphene samples, the evaluation of the location of defects is difficult because the position of the D mode is the same for both graphene layers. However, with the help of isotope labeling, one can distinguish between the defects in the top and in the bottom layers. Figure 10 shows the Raman spectrum of turbostratic graphene and AB-stacked graphene bilayers after the creation of defects by oxygen plasma. It can be seen that the D mode appears both for the top and bottom layers. As the conditions of the creation of defects only in the top graphene layer, it was concluded that the defects in the top layer can

scatter the phonons in the bottom layer.[43] The scattering of the phonons is more efficient for the AB-stacked graphene because the layers interact more efficiently. The scattering of the phonons by defects in the neighboring layer has very important consequences for the evaluation of the number of defects in graphene samples using D mode intensity in the Raman spectra. For graphene multilayers, the number of defects is overestimated by 45% and 20% in the case of AB-stacked and turbostratic stacking of layers, respectively.

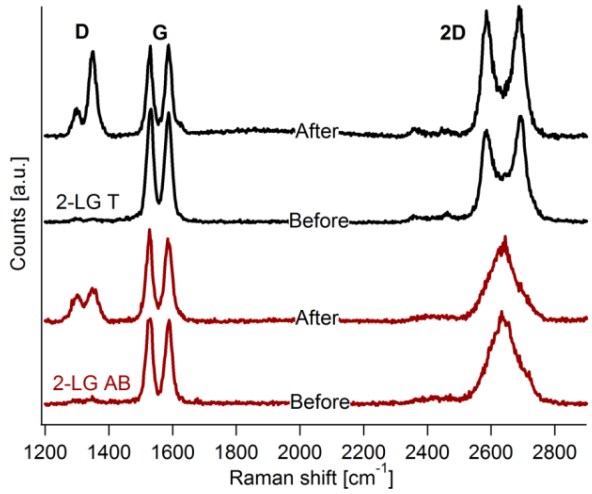

Figure 10. Raman spectra of the T-2-LG and AB-2-LG after the creation of defects by oxygen plasma.[43]

3.6 Functionalization of isotopically labeled graphene

Functionalized graphene is a promising component of graphene sandwiches because the functionalization can add new functionality to graphene, but it may not affect the morphology of other graphene layers significantly. Isotopic labeling of the graphene allows directly addressing the properties and the changes in individual components of these sandwiches. 2-LG can also serve as a model system to study the role of the substrate in graphene reactivity. The 2-LG can be viewed as graphene on a graphene substrate. Furthermore, in this case, one can also evaluate a role of the specific orientation of graphene with respect to the substrate by comparing the reactivity of T-2-LG and AB-2-LG. To avoid interference of different effects and contamination one needs to select an appropriate test reaction. Graphene can be functionalized by several different routes, but most of them are realized in the liquid phase.[44]

This represents a problem because the graphene surface can be easily contaminated even if ultrahigh purity solvents are used. Therefore, it is more convenient to select a reaction in the gas phase. In this case, the most suitable reaction seems to be fluorination using XeF_2.[45] In comparison to oxidation, this reaction is easier to control and also it is easier to characterize reaction products. To ensure the same conditions for comparison of the reactivity of graphene on different substrates, we fluorinated the sample, which contained single-layer graphene, T-2-LG and AB-2-LG all placed on Si/SiO_2 substrate. The reactivity of graphene can be easily evaluated by Raman spectroscopy, because the higher fluorination level corresponds to the stronger D mode in the Raman spectrum. The comparison of the Raman spectra before and after fluorination is shown in Figure 11. The highest reactivity exhibits single-layer graphene (representing graphene on Si/SiO_2 substrate), which is demonstrated by the strong D mode after the reaction. Smaller reactivity is found in the case of the T-2-LG, which represents a graphene-on-graphene substrate.[46] The smallest reactivity is found in case of the AB-2-LG. These results demonstrate the importance of graphene–substrate orientation for the reactivity of graphene. The stronger interactions in the case of the AB-2-LG corresponds to the lower reactivity as compared with weaker interactions in the case of T-2-LG. It is worth mentioning that in the case of 2-LG, we observed also the D mode of the bottom graphene layer. However, this does not mean that the bottom layer is fluorinated. (Note that graphene fluorination was used to identify the position of add-layers grown on single-layer graphene as only the top layer is expected to be fluorinated.[47])

The D mode in these cases comes from the interaction of phonons in the bottom layer with defects in the top layer. Thanks to isotope labeling, we can distinguish between the D mode of the top layer and bottom layer, consequently, the results are not affected by a contribution of the bottom layer phonon–defects interactions. In the case of the 2-LG, the isotope labeling also enables disentangling the effects of the functionalization on doping of the top and bottom layers. These effects, however, have to be studied using Raman mapping to avoid local inhomogeneities.

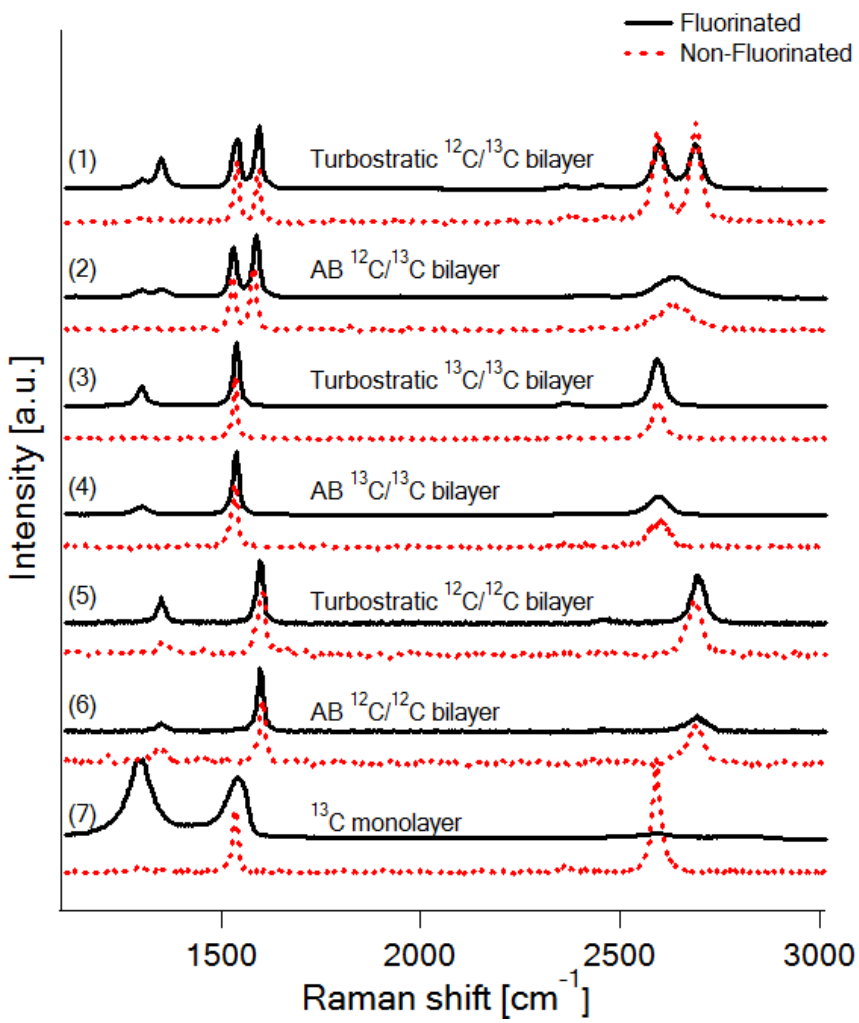

Figure 11. Raman spectra of the 1-LG, and isotopically labeled of the T-2-LG and AB-2-LG before and after fluorination. The figure was adopted from Ref.[46]

Figure 12 shows the distribution of the G mode frequencies of the top graphene layer before and after fluorination. The frequency of the G mode is obviously increased after fluorination. This is in line with the expectation as the fluorine functional group is withdrawing electrons from graphene. The effect is slightly more pronounced for the T-2-LG, which corresponds to higher fluorine content. Figure 13 shows the distribution of the G mode frequencies for the bottom graphene layer. In the case of the T-2-LG, the G mode of the bottom layer is upshifted similarly to that of the top layer. On the other hand, for the AB-2-LG, there is almost no shift. This actually resembles the behavior of the AB-2-LG during the electrochemical doping and points to almost no charge transfer between the top and bottom layers in AB-2-LG.

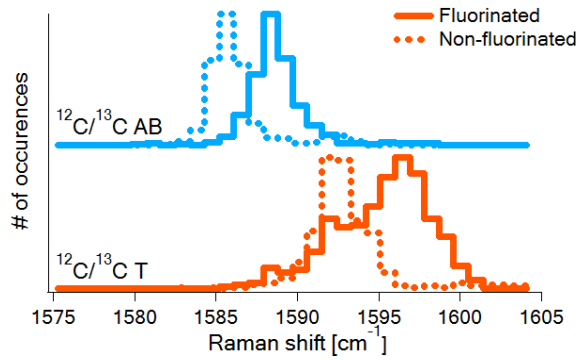

Figure 12. Histograms of the G mode frequencies of the ^{12}C top layer for the non-fluorinated and fluorinated isotopically labeled 2-LG. The figure was adopted from Ref.[46]

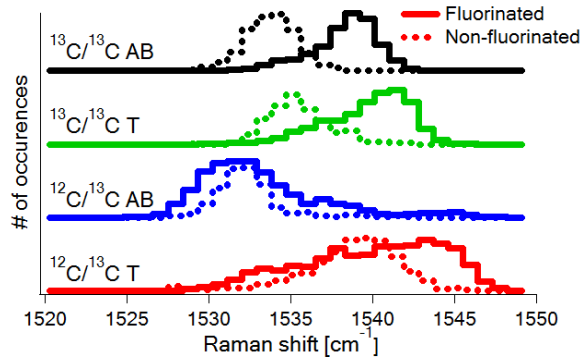

Figure 13. Histograms of the G mode frequencies of the ^{13}C bottom layer for the non-fluorinated and fluorinated isotopically labeled 2-LG. The figure was adopted from Ref.[46]

The formation of the graphene sandwiches usually includes thermal treatment, which is necessary to remove polymer used for the transfer process. Therefore, it is important to study the effects of temperature on functionalized graphene. For our study, we used fluorinated graphene.[46,48] The samples were prepared by the reaction of isotopically labeled graphene with XeF_2. The temperature treatment was performed in the Raman cell, which allowed controlled heating in the inert atmosphere and simultaneous measurement of the Raman spectra. Raman spectroscopy was applied to monitor changes in the functionalization of

graphene, the changes in the doping, changes in the stress of the graphene layer and the formation of defects. We compared also monolayer and bilayer stability. It was found that although the graphene bilayer is significantly less reactive than the monolayer, the decomposition process occurs at similar temperatures for both materials. This has important implications for the formation of sandwiches by the subsequent transfer of the components.

3.7 Spacer for measurements of Surface enhanced Raman spectroscopy (SERS)

Isotopically labeled graphene bilayers can be used to study the effects of the spacer on the enhancement of the Raman signal enhancement in SERS experiments. Figure 14 shows the sandwich heterostructure consisting of the ^{12}C graphene layer, ^{13}C graphene layer and 15 nm of gold layer, together with the Raman spectrum of this heterostructure. The signal of graphene covered by gold is significantly enhanced. However, as can be observed in Figure 14, the signal of the graphene layer closer to the gold layer is stronger than the signal of the layer, which is further away. This is in contrast to the uncovered graphene, where the intensity of the G mode of the top and bottom layers is similar. A more detailed analysis shows that the change of the signal intensity corresponds to the decrease of the electromagnetic field generated by a gold plasmon at the distance of about 0.34 nm from the layer next to the gold layer. Moreover, Raman mapping of the samples shows that the change of the signal intensity is homogeneous within the measured area.

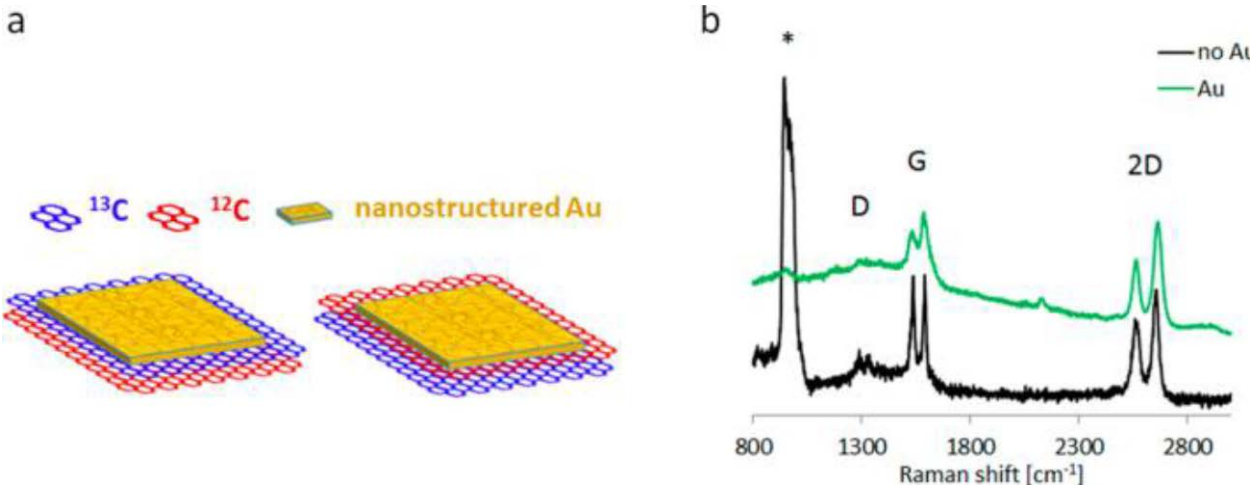

Figure 14. Left: Schematic image of the 2-LG–gold heterostructure. Right: Raman spectra of the 2-LG before after deposition of the gold layer. The Raman spectrum of 2-LG before gold deposition is multiplied by a factor of 100. The figure was adopted from Ref.[49]

3.8 Sandwich structures based on isotopically labeled graphene

Graphene bilayer can be used as a host structure for other materials. For example, fullerenes can be placed between two graphene layers to form a so-called 2-D peapod.[50,51] The structure is asymmetric by means of doping because the bottom layer is in contact with the substrate and the top layer is in contact with the environment. Consequently, the properties of the top layer and bottom layer are different. Using isotope labeling, it is possible to disentangle the strain and the doping in such a sandwich material. Furthermore, the interaction between host and guest material can be tuned. For example, simple temperature treatment leads to changes in the strain and doping with magnitude specific to the layer position with respect to the substrate. Figure 15 shows the development of doping and strain in the top and bottom graphene layers for the $^{12}C/C_{70}/^{13}C$ heterostructure. Figure 15 shows the strain and doping level dependence for the heterostructure in dependence on temperature. The top layer is more relaxed and this does not change with the temperature. The doping is larger for the bottom layer also at all temperatures. While for the top layer it remains almost constant in the probed temperature range, for the bottom layer it slightly increases with decreasing temperature.[51]

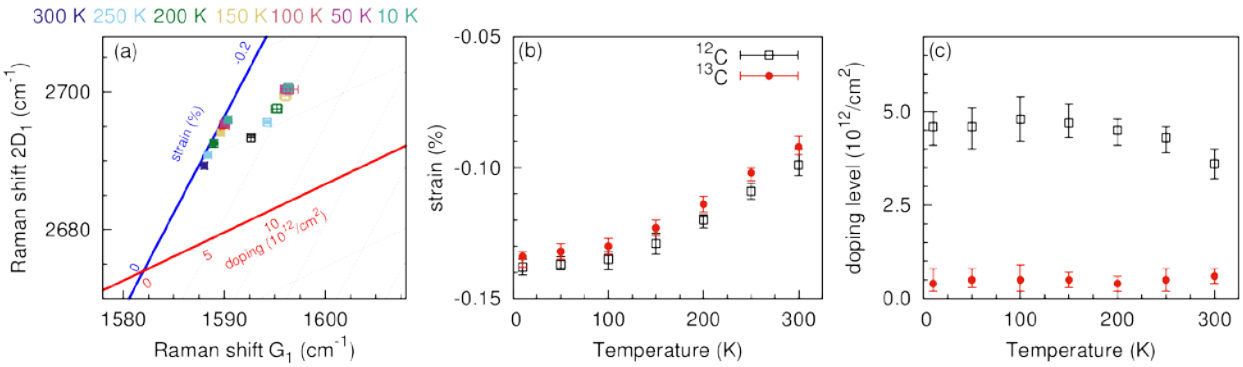

Figure 15. An analysis of the behavior of the $^{12}C/C_{70}/^{13}C$ heterostructure in dependence on the temperature. a) A plot of the G/2D mode positions for the doping strain analysis. b) Strain dependence on temperature. c) Plot of the doping level dependence on the temperature. The figure was adopted from Ref.[51]

4 Conclusions and outlook

Graphene and 2-D materials in general can also be viewed as base components for the building of new classes of materials with novel properties. The ability to tune the coveted properties of these components by external stimuli and addressing precisely the resulting electronic structure of these components is expected to contribute to a revolution in nanoscience and nanotechnology in upcoming years.

Advanced Raman spectroscopy investigation was demonstrated to be an extremely useful tool to study the graphene and the graphene-based structures. The capability of Raman spectroscopy can be further extended to studies of multilayer systems by using the isotope labeling, which enables addressing individual graphene layers. This unique approach has the power to uncover distribution of the doping, strain or defect formation in multilayer graphene samples. Application of the isotope labeling was successfully demonstrated on 2-LG, but the methodology can be extended to an arbitrary number of layers providing that the Raman peaks of different layers can be resolved conveniently.

The Raman spectroscopy was also put in synergy with other techniques. This is represented for example by *in situ* heating or in situ doping of the graphene structures. Both the heating and the intended doping modify the properties of graphene, and Raman spectroscopy can directly monitor these changes. A combination of the doping experiments and Raman spectroscopy leads to new important discoveries, including canceling of the interfering electronic transitions. Again, such *in situ* studies can be extended by measuring the Raman spectra with the application of external magnetic field, application of the gate voltage or measurements in different atmospheres (vacuum, oxygen, hydrogen, etc.)

Further challenges represent the use of isotope labeling to study modified/functionalized graphene samples or heterostructures based on graphene and other 2-D materials. This work provided proof of concept by employing fluorination of 2-LG in the gas phase, where the reactivity and doping was successfully investigated. The importance of the study is given by its outreach to many different chemical reactions, which can be further studied on the graphene or the graphene combined with other 2-D materials. In the latter case, the 2-D material(s) may not respond strongly to the external effects (like doping), but the graphene can be used as a probe, which would sense the doping/strain variations.

Regarding the future prospects, the 2-D materials are the fixed stars of current scientific and technological efforts and the obtained knowledge summarized in this thesis has significantly contributed to the field. Further directions of the ongoing research aim to development of optoelectronic and sensing devices, as well as to address the physics of unconventional condensed phases by Raman spectroscopy at extreme conditions. Very recently, new concepts profiting from the stacking degrees of freedom, like pseudospintronics and twistronics have been introduced, thus the expertize presented in this work has a significant potential to promote considerable progress both in the fundamental and technological playground.

5 References

1. Cao, Y.; Fatemi, V.; Fang, S.; Watanabe, K.; Taniguchi, T.; Kaxiras, E.; Jarillo-Herrero, P. Unconventional superconductivity in magic-angle graphene superlattices. *Nature* **2018,** *556* (7699), 43-50.

2. Novoselov, K. S.; Geim, A. K.; Morozov, S. V.; Jiang, D.; Katsnelson, M. I.; Grigorieva, I. V.; Dubonos, S. V.; Firsov, A. A. Two-dimensional gas of massless Dirac fermions in graphene. *Nature* **2005,** *438* (7065), 197-200.

3. Li, X. S.; Cai, W. W.; An, J. H.; Kim, S.; Nah, J.; Yang, D. X.; Piner, R.; Velamakanni, A.; Jung, I.; Tutuc, E.; Banerjee, S. K.; Colombo, L.; Ruoff, R. S. Large-Area Synthesis of High-Quality and Uniform Graphene Films on Copper Foils. *Science* **2009,** *324* (5932), 1312-1314.

4. Reina, A.; Jia, X. T.; Ho, J.; Nezich, D.; Son, H. B.; Bulovic, V.; Dresselhaus, M. S.; Kong, J. Large Area, Few-Layer Graphene Films on Arbitrary Substrates by Chemical Vapor Deposition. *Nano Letters* **2009,** *9* (1), 30-35.

5. Gao, L.; Guest, J. R.; Guisinger, N. P. Epitaxial Graphene on Cu(111). *Nano Letters* **2010,** *10* (9), 3512-3516.

6. Reina, A.; Son, H.; Jiao, L.; Fan, B.; Dresselhaus, M. S.; Liu, Z.; Kong, J. Transferring and Identification of Single- and Few-Layer Graphene on Arbitrary Substrates. *J. Phys. Chem. C* **2008,** *112* (46), 17741-17744.

7. Saito, R.; Jorio, A.; Souza, A. G.; Dresselhaus, G.; Dresselhaus, M. S.; Pimenta, M. A. Probing phonon dispersion relations of graphite by double resonance Raman scattering. *Phys. Rev. Lett.* **2002,** *88* (2), 027401.

8. Das, A.; Pisana, S.; Chakraborty, B.; Piscanec, S.; Saha, S. K.; Waghmare, U. V.; Novoselov, K. S.; Krishnamurthy, H. R.; Geim, A. K.; Ferrari, A. C.; Sood, A. K. Monitoring dopants by Raman scattering in an electrochemically top-gated graphene transistor. *Nat. Nanotechnol.* **2008,** *3* (4), 210-215.

9. Yan, J.; Zhang, Y. B.; Kim, P.; Pinczuk, A. Electric field effect tuning of electron-phonon coupling in graphene. *Phys. Rev. Lett.* **2007,** *98* (16), 166802.

10. Zhu, J.; Jhaveri, R.; Woo, J. C. S. The effect of traps on the performance of graphene field-effect transistors. *Appl. Phys. Lett.* **2010,** *96* (19), 193503.

11. Kalbac, M.; Reina-Cecco, A.; Farhat, H.; Kong, J.; Kavan, L.; Dresselhaus, M. S. The Influence of Strong Electron and Hole Doping on the Raman Intensity of Chemical Vapor-Deposition Graphene. *Acs Nano* **2010,** *4* (10), 6055-6063.

12. Frank, O.; Dresselhaus, M. S.; Kalbac, M. Raman spectroscopy and in situ Raman spectroelectrochemistry of isotopically engineered graphene systems. *Acc. of Chem. Res.* **2015,** *48* (1), 111-118.

13. Lazzeri, M.; Mauri, F. Nonadiabatic Kohn anomaly in a doped graphene monolayer. *Phys. Rev. Lett.* **2006,** *97* (26), 266407.

14. Kominkova, Z.; Kalbac, M. Raman spectroscopy of strongly doped CVD-graphene. *Phys. Status Solidy B* **2013,** *250* (12), 2659-2661.

15. Basko, D. M. Calculation of the Raman G peak intensity in monolayer graphene: role of Ward identities. *New. J. Phys.* **2009,** *11*, 095011.

16. Basko, D. M.; Piscanec, S.; Ferrari, A. C. Electron-electron interactions and doping dependence of the two-phonon Raman intensity in graphene. *Phys. Rev. B* **2009,** *80* (16), 165413.

17. Banerjee, S. K.; Register, L. F.; Tutuc, E.; Reddy, D.; MacDonald, A. H. Bilayer PseudoSpin Field-Effect Transistor (BiSFET): A Proposed New Logic Device. *Ieee Electron Device Letters* **2009,** *30* (2), 158-160.

18. Kominkova, Z.; Kalbac, M. Extreme electrochemical doping of a graphene-polyelectrolyte heterostructure. *Rsc Advances* **2014,** *4* (22), 11311-11316.

19. Kalbac, M.; Kong, J.; Dresselhaus, M. S. Doping of bi-layer graphene by gradually polarizing a ferroelectric polymer. *Phys. Status Solidy B* **2013,** *250* (12), 2649-2652.

20. Si, C.; Sun, Z. M.; Liu, F. Strain engineering of graphene: a review. *Nanoscale* **2016,** *8* (6), 3207-3217.

21. Levy, N.; Burke, S. A.; Meaker, K. L.; Panlasigui, M.; Zettl, A.; Guinea, F.; Neto, A. H. C.; Crommie, M. F. Strain-Induced Pseudo-Magnetic Fields Greater Than 300 Tesla in Graphene Nanobubbles. *Science* **2010,** *329* (5991), 544-547.

22. Lee, J. E.; Ahn, G.; Shim, J.; Lee, Y. S.; Ryu, S. Optical separation of mechanical strain from charge doping in graphene. *Nature Comm.* **2012,** *3, 1024*.

23. del Corro, E.; Kavan, L.; Kalbac, M.; Frank, O. Strain Assessment in Graphene Through the Raman 2D ' Mode. *J. Phys. Chem. C* **2015,** *119* (45), 25651-25656.

24. Frank, O.; Vejpravova, J.; Holy, V.; Kavan, L.; Kalbac, M. Interaction between graphene and copper substrate: The role of lattice orientation. *Carbon* **2014,** *68*, 440-451.

25. Costa, S. D.; Weis, J. E.; Frank, O.; Kalbac, M. Temperature and face dependent copper-graphene interactions. *Carbon* **2015,** *93*, 793-799.

26. Costa, S. D.; Weis, J. E.; Frank, O.; Fridrichova, M.; Kalbac, M. Monitoring the doping of graphene on SiO2/Si substrates during the thermal annealing process. *Rsc Advances* **2016,** *6* (76), 72859-72864.

27. Bonini, N.; Lazzeri, M.; Marzari, N.; Mauri, F. Phonon anharmonicities in graphite and graphene. *Phys. Rev. Lett.* **2007,** *99* (17), 176802.

28. Verhagen, T.; Vales, V.; Frank, O.; Kalbac, M.; Vejpravova, J. Temperature-induced strain release via rugae on the nanometer and micrometer scale in graphene monolayer. *Carbon* **2017,** *119*, 483-491.

29. Verhagen, T.; Vales, V.; Kalbac, M.; Vejpravova, J. Electronic and mechanical response of graphene on BaTiO3 at martensitic phase transitions. *J. Phys.-Condensed Matter* **2018,** *30* (8), 085001.

30. Kalbac, M.; Frank, O.; Kong, J.; Sanchez-Yamagishi, J.; Watanabe, K.; Taniguchi, T.; Jarillo-Herrero, P.; Dresselhaus, M. S. Large Variations of the Raman Signal in the Spectra of Twisted Bilayer Graphene on a BN Substrate. *J. Phys. Chem. Lett.* **2012,** *3* (6), 796-799.

31. Kalbac, M.; Kong, J.; Dresselhaus, M. S. Raman Spectroscopy as a Tool to Address Individual Graphene Layers in Few-Layer Graphene. *J. Phys. Chem. C* **2012,** *116* (35), 19046-19050.

32. del Corro, E.; Kalbac, M.; Fantini, C.; Frank, O.; Pimenta, M. Isotopic C-13/C-12 effect on the resonant Raman spectrum of twisted bilayer graphene. *Phys. Rev. B* **2013,** *88* (15), 155436.

33. Kalbac, M.; Kong, J.; Kavan, L.; Dresselhaus, M. S. Raman spectroscopy of isotopically labeled two-layer graphene. *Phys. Status Solidy B* **2012,** *249* (12), 2500-2502.

34. Frank, O.; Kavan, L.; Kalbac, M. Carbon isotope labelling in graphene research. *Nanoscale* **2014,** *6* (12), 6363-6370.

35. Kalbac M; Frank, O.; Kavan, L. The control of graphene double-layer formation in copper-catalyzed chemical vapor deposition. *Carbon* **2012,** *50*, 3682-3687.

36. Costa, S. D.; Weis, J. E.; Frank, O.; Fridrichova, M.; Kalbac, M. Addressing Raman features of individual layers in isotopically labeled Bernal stacked bilayer graphene. *2D Mat.* **2016,** *3* (2), 025022.

37. Araujo, P. T.; Frank, O.; Mafra, D. L.; Fang, W.; Kong, J.; Dresselhaus, M. S.; Kalbac, M. Mass-related inversion symmetry breaking and phonon self-energy renormalization in isotopically labeled AB-stacked bilayer graphene. *Sci. Rep.* **2013,** *3,* 2061.

38. Kalbac, M.; Farhat, H.; Kong, J.; Janda, P.; Kavan, L.; Dresselhaus, M. S. Raman spectroscopy and in situ Raman spectroelectrochemistry of bi-layer 12C/13C graphene. *Nano Letters* **2011,** *11* (5), 1957-1963.

39. Kalbac M; Frank, O.; Kavan, L. Effects of heat treatment on Raman spectra of two-layer 12C/13C graphene. *Chem. -Eur. J.* **2013,** *18* (43), 13877-13884.

40. Ek-Weis, J.; Costa, S.; Frank, O.; Kalbac, M. Heating Isotopically Labeled Bernal Stacked Graphene: A Raman Spectroscopy Study. *J. Phys. Chem. Lett.* **2014,** *5* (3), 549-554.

41. Kalbac M; Lehtinen, O.; Krasheninnikov, A. V.; Keinonen, J. Ion-Irradiation-Induced Defects in Isotopically-Labeled Two Layered Graphene:

Enhanced In-Situ Annealing of the Damage. *Adv. Mat.* **2013,** 25(7), 1004-1009.

42. Jorio, A.; Lucchese, M. M.; Stavale, F.; Ferreira, E. H. M.; Moutinho, M. V. O.; Capaz, R. B.; Achete, C. A. Raman study of ion-induced defects in N-layer graphene. *J. Phys.-Condensed Matter* **2010,** *22* (33), 334204.

43. Costa, S. D.; Weis, J. E.; Frank, O.; Kalbac, M. Effect of layer number and layer stacking registry on the formation and quantification of defects in graphene. *Carbon* **2016,** *98*, 592-598.

44. Paulus, G. L.; Wang, Q. H.; Strano, M. S. Covalent Electron Transfer Chemistry of Graphene with Diazonium Salts. *Acc. Chem. Res.* **2013,** *46* (1), 160-170.

45. Nair, R. R.; Ren, W.; Jalil, R.; Riaz, I.; Kravets, V. G.; Britnell, L.; Blake, P.; Schedin, F.; Mayorov, A. S.; Yuan, S.; Katsnelson, M. I.; Cheng, H. M.; Strupinski, W.; Bulusheva, L. G.; Okotrub, A. V.; Grigorieva, I. V.; Grigorenko, A. N.; Novoselov, K. S.; Geim, A. K. Fluorographene: A Two-Dimensional Counterpart of Teflon. *Small* **2010,** *6* (24), 2877-2884.

46. Weis, J. E.; Costa, S. D.; Frank, O.; Bastl, Z.; Kalbac, M. Fluorination of Isotopically Labeled Turbostratic and Bernal Stacked Bilayer Graphene. *Chem. -Eur. J.* **2015,** *21* (3), 1081-1087.

47. Fang, W. J.; Hsu, L. A.; Caudillo, R.; Song, Y.; Birdwell, A. G.; Zakar, E.; Kalbac, M.; Palacios, T.; Dresselhaus, M. S.; Araujo, P. T.; Kong, J. Rapid Identification of Stacking Orientation in Isotopically Labeled Chemical-Vapor Grown Bilayer Graphene by Raman Spectroscopy. *Nano Letters* **2013,** 13(4), 1541-1548.

48. Costa, S. D.; Weis, J. E.; Frank, O.; Bastl, Z.; Kalbac, M. Thermal treatment of fluorinated graphene: An in situ Raman spectroscopy study. *Carbon* **2015,** *84*, 347-354.

49. Weis, J. E.; Costa, S.; Frank, O.; Fridrichova, M.; Vlckova, B.; Vejpravova, J.; Kalbac, M. SERS of Isotopically Labeled C-12/C-13 Graphene Bilayer-Gold Nanostructured Film Hybrids: Graphene Layer as Spacer and SERS Probe. *J. Phys. Chem. C* **2017,** *121* (21), 11680-11686.

50. Vales, V.; Verhagen, T.; Vejpravova, J.; Frank, O.; Kalbac, M. Addressing asymmetry of the charge and strain in a two-dimensional fullerene peapod. *Nanoscale* **2016,** *8* (2), 735-740.

51. Verhagen, T. G. A.; Vales, V.; Kalbac, M.; Vejpravova, J. Temperature-induced evolution of strain and doping in an isotopically labeled two-dimensional graphene-C-70 fullerene peapod. *Diamond and Rel. Mat.* **2017,** *75*, 140-145.

6 List of the commented publications:

1) Kalbac, M.; Reina-Cecco, A.; Farhat, H.; Kong, J.; Kavan, L.; Dresselhaus, M. S. The Influence of Strong Electron and Hole Doping on the Raman Intensity of Chemical Vapor-Deposition Graphene. *Acs Nano* **2010**, 4 (10), 6055-6063.

2) Frank, O.; Dresselhaus, M. S.; Kalbac, M. Raman spectroscopy and in situ Raman spectroelectrochemistry of isotopically engineered graphene systems. *Acc. Chem. Res.* **2015**, 48 (1), 111-118.

3) Kominkova, Z.; Kalbac, M. Raman spectroscopy of strongly doped CVD-graphene. *Phys. Status Solidy B* **2013**, 250 (12), 2659-2661.

4) Kominkova, Z.; Kalbac, M. Extreme electrochemical doping of a graphene-polyelectrolyte heterostructure. *Rsc Advances* **2014**, 4 (22), 11311-11316.

5) Kalbac, M.; Kong, J.; Dresselhaus, M. S. Doping of bi-layer graphene by gradually polarizing a ferroelectric polymer. *Phys. Status Solidy B* **2013**, 250 (12), 2649-2652.

6) del Corro, E.; Kavan, L.; Kalbac, M.; Frank, O. Strain Assessment in Graphene Through the Raman 2D ' Mode. *J. Phys. Chem. C* **2015**, 119 (45), 25651-25656.

7) Frank, O.; Vejpravova, J.; Holy, V.; Kavan, L.; Kalbac, M. Interaction between graphene and copper substrate: The role of lattice orientation. *Carbon* **2014**, 68, 440-451.

8) Costa, S. D.; Weis, J. E.; Frank, O.; Kalbac, M. Temperature and face dependent copper-graphene interactions. *Carbon* **2015**, 93, 793-799.

9) Costa, S. D.; Weis, J. E.; Frank, O.; Fridrichova, M.; Kalbac, M. Monitoring the doping of graphene on SiO_2/Si substrates during the thermal annealing process. *Rsc Advances* **2016**, 6 (76), 72859-72864.

10) Verhagen, T.; Vales, V.; Frank, O.; Kalbac, M.; Vejpravova, J. Temperature-induced strain release via rugae on the nanometer and micrometer scale in graphene monolayer. *Carbon* **2017**, 119, 483-491.

11) Verhagen, T.; Vales, V.; Kalbac, M.; Vejpravova, J. Electronic and mechanical response of graphene on BaTiO3 at martensitic phase transitions. *J. Phys.-Cond. Matt.* **2018**, 30 (8), 085001.

12) Kalbac, M.; Frank, O.; Kong, J.; Sanchez-Yamagishi, J.; Watanabe, K.; Taniguchi, T.; Jarillo-Herrero, P.; Dresselhaus, M. S. Large Variations of the Raman Signal in the Spectra of Twisted Bilayer Graphene on a BN Substrate. *J. Phys. Chem. Lett.* **2012**, 3 (6), 796-799.

13) Kalbac, M.; Kong, J.; Dresselhaus, M. S. Raman Spectroscopy as a Tool to Address Individual Graphene Layers in Few-Layer Graphene. *J. Phys. Chem. C* **2012**, 116 (35), 19046-19050.

14) del Corro, E.; Kalbac, M.; Fantini, C.; Frank, O.; Pimenta, M. Isotopic C-13/C-12 effect on the resonant Raman spectrum of twisted bilayer graphene. *Phys. Rev. B* **2013**, 88 (15), 155436.

15) Kalbac, M.; Kong, J.; Kavan, L.; Dresselhaus, M. S. Raman spectroscopy of isotopically labeled two-layer graphene. *Phys. Status Solidy B* **2012**, 249 (12), 2500-2502.

16) Frank, O.; Kavan, L.; Kalbac, M. Carbon isotope labelling in graphene research. *Nanoscale* **2014**, 6 (12), 6363-6370.

17) Kalbac M; Frank, O.; Kavan, L. The control of graphene double-layer formation in copper-catalyzed chemical vapor deposition. *Carbon* **2012**, 50, 3682-3687.

18) Costa, S. D.; Weis, J. E.; Frank, O.; Fridrichova, M.; Kalbac, M. Addressing Raman features of individual layers in isotopically labeled Bernal stacked bilayer graphene. *2D Mat.* **2016**, 3 (2), 025022.

19) Araujo, P. T.; Frank, O.; Mafra, D. L.; Fang, W.; Kong, J.; Dresselhaus, M. S.; Kalbac, M. Mass-related inversion symmetry breaking and phonon self-energy renormalization in isotopically labeled AB-stacked bilayer graphene. *Sci. Rep.* **2013**, 3, 2061.

20) Kalbac, M.; Farhat, H.; Kong, J.; Janda, P.; Kavan, L.; Dresselhaus, M. S. Raman spectroscopy and in situ Raman spectroelectrochemistry of bi-layer 12C/13C graphene. *Nano Letters* **2011**, 11 (5), 1957-1963.

21) Kalbac M; Frank, O.; Kavan, L. Effects of heat treatment on Raman spectra of two-layer 12C/13C graphene. *Chem. -Eur. J.* **2013**, 18 (43), 13877-13884.

22) Ek-Weis, J.; Costa, S.; Frank, O.; Kalbac, M. Heating Isotopically Labeled Bernal Stacked Graphene: A Raman Spectroscopy Study. *J. Phys. Chem. Lett.* **2014**, 5 (3), 549-554.

23) Kalbac M; Lehtinen, O.; Krasheninnikov, A. V.; Keinonen, J. Ion-Irradiation-Induced Defects in Isotopically-Labeled Two Layered Graphene: Enhanced In-Situ Annealing of the Damage. *Adv. Mat.* **2013**, 25(7)1004-1009.

24) Costa, S. D.; Weis, J. E.; Frank, O.; Kalbac, M. Effect of layer number and layer stacking registry on the formation and quantification of defects in graphene. *Carbon* **2016**, 98, 592-598.

25) Weis, J. E.; Costa, S. D.; Frank, O.; Bastl, Z.; Kalbac, M. Fluorination of Isotopically Labeled Turbostratic and Bernal Stacked Bilayer Graphene. *Chem. -Eur. J.* **2015**, 21 (3), 1081-1087.

26) Fang, W. J.; Hsu, L. A.; Caudillo, R.; Song, Y.; Birdwell, A. G.; Zakar, E.; Kalbac, M.; Palacios, T.; Dresselhaus, M. S.; Araujo, P. T.; Kong, J. Rapid Identification of Stacking Orientation in Isotopically Labeled Chemical-Vapor Grown Bilayer Graphene by Raman Spectroscopy. *Nano Letters* **2013**, 13(4), 1541-1548.

27) Costa, S. D.; Weis, J. E.; Frank, O.; Bastl, Z.; Kalbac, M. Thermal treatment of fluorinated graphene: An in situ Raman spectroscopy study. *Carbon* **2015**, 84, 347-354.

28) Weis, J. E.; Costa, S.; Frank, O.; Fridrichova, M.; Vickova, B.; Vejpravova, J.; Kalbac, M. SERS of Isotopically Labeled C-12/C-13 Graphene Bilayer-Gold Nanostructured Film Hybrids: Graphene Layer as Spacer and SERS Probe. *J. Phys. Chem. C* **2017**, 121 (21), 11680-11686.

29) Vales, V.; Verhagen, T.; Vejpravova, J.; Frank, O.; Kalbac, M. Addressing asymmetry of the charge and strain in a two-dimensional fullerene peapod. *Nanoscale* **2016**, 8 (2), 735-740.

30) Verhagen, T. G. A.; Vales, V.; Kalbac, M.; Vejpravova, J. Temperature-induced evolution of strain and doping in an isotopically labeled two-dimensional graphene-C-70 fullerene peapod. *Diamond and Rel. Mat.* **2017**, 75, 140-145.

Appendix 1

Collection of the commented publications: